Preliminary Exam Write-up

Abhishek Hingrajiya

February 1, 2025

1 Introduction

Quantum chromodynamics is a theory of strongly interacting particles like quarks and gluons. Quarks and gluons are fundamental particles that makeup hadrons like protons and neutrons. Quarks and gluons can only be produced at very high energy for a very short time. Particle colliders like the Relativistic Heavy Ion Collider(RHIC) and the Large Hadron Collider(LHC) can produce extremely high energy by colliding heavy ions like Pb and Au at ultra-relativistic energy. The collisions of heavy ions produced a novel state of matter known as Quark Gluon Plasma (QGP).

1.1 Quantum Chromodynamics (QCD)

Strong interaction is mediated by the exchange of gluon, a vector gauge boson, between quarks and other gluons. The Lagrangian for QCD is as follows

$$\mathcal{L} = i\bar{\psi}\gamma^{\mu}D_{\mu}\psi - \frac{1}{4}G^{a}_{\mu\nu}G^{\mu\nu}_{a} \tag{1}$$

Interaction between quarks and gluons, collectively known as partons, occurs via three color charges: red, green, and blue. The interaction strength depends on the coupling constant α_s. The coupling constant decreases as momentum transfer (Q) increases, as shown in equation(2)

$$\alpha_S(Q^2) \propto \frac{1}{\ln\left[\frac{Q^2}{\Lambda_{\mathrm{QCD}}}\right]} \tag{2}$$

At low momentum transfers, the coupling is strong and can be handled by lattice QCD. At large momentum transfers, the coupling constant would become smaller. At weak coupling limit ($\alpha_s << 1$), momentum transfer (Q^2) is massive and temperature is high. This region of QCD is handled by perturbative QCD. As momentum transfer keeps increasing, the coupling gets weaker. This allows quarks and gluons to be free at higher energy within the medium. This is called *Asymptotic Freedom*. Figure (1) shows that increasing momentum transfer weakens the coupling.

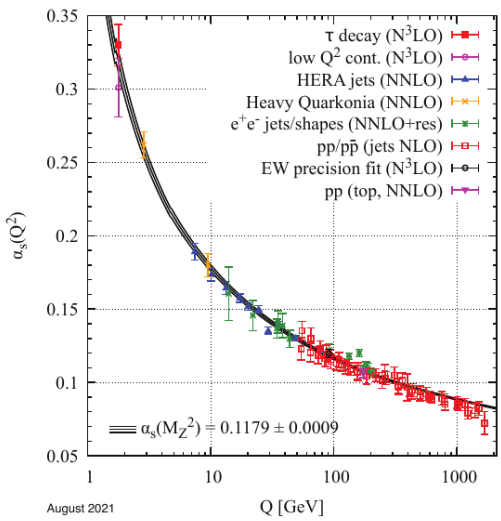

Figure 1: Measurement of α_s at different energy[16]

J.D. Bjorken predicted that QGP could be produced for a time scale of $\geq$ 5fm/c at a temperature of 200-300 MeV.[8]. Particle colliders can achieve these extreme energies by accelerating charged heavy ions like Pb or Au to 99% speed of light by the electromagnetic field. The first confirmed

production of QGP was noted by the Relativistic Heavy Ion Collider (RHIC) at Brookhaven National Laboratory.[17]

1.2 Phases transition in QCD

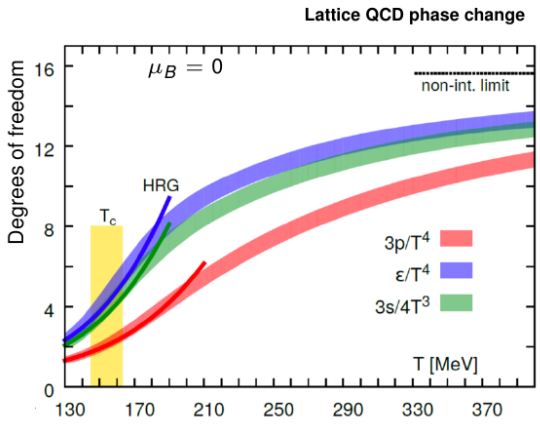

(a) Normalized pressure, energy density, and entropy density as a function of the temperature. Crossover transition at $T_c = 154 \pm 9MeV$ [7]

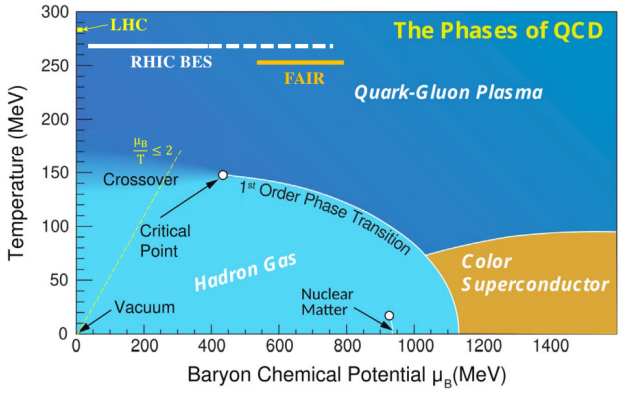

(b) QCD Phase space diagram as a function of baryon chemical potential.[5]

Figure 2: Phase transition in QCD

Perturbative QCD helps study large momentum transfer processes, but it breaks down in the phase space of QGP. In this case, lattice QCD calculations help explore the nature of bound state hadrons. In Figure (2a), lattice calculations done at $\mu_B = 0$ show a sharp but continuous rise in pressure (p), energy density (ϵ), and entropy (s) at a critical temperature of 155 MeV. The increase in the thermodynamic quantities is an indication of phase transition. An increase in degrees of freedom arises from the deconfinement of quarks and gluons.
The zero baryon chemical potential ($\mu_B = 0$) implies number of quarks and anti-quarks are same. This is a good approximation for a heavy-ion collision at particle colliders. Hence, particle colliders, like LHC and RHIC, provide a unique opportunity to study QGP phases.

1.3 Time Evolution for QGP

The time evolution of QGP in heavy ion collision is shown in Figure(3). A summary of each stage is presented below.

1. Initial State : Two heavy nuclei are accelerated close to the speed of light. Both nuclei turn into disks due to Lorentz contraction. The initial state will be determined by how long it takes for the two nuclei to collide. This can be calculated by

$$t = \frac{R}{\gamma}$$

R is the radius of nuclei. For Pb R = 14 fm. γ is the relativistic factor. In the case of Pb-Pb collision at 5.02 TeV, the value of $\gamma = 2400$.

2. Thermalization : After the collision, an immense amount of energy is deposited in a very short period in a small volume. After some time of 1 fm/c following a head-on collision, the energy density in a small area is of the order of ≈ 10 $textsGeV/\text{fm}^3$. The high energy density provides a suitable environment for the formation of QGP. After the formation of QGP, the

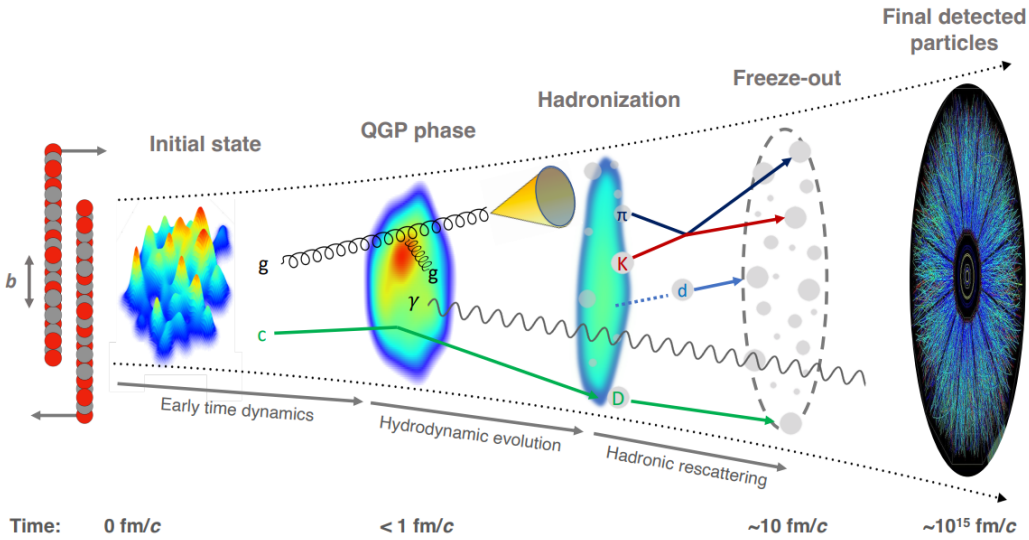

Figure 3: Time Evolution of QGP in heavy ion collision [5]

system thermalizes in 1 fm/c time.

3. Hydrodynamic Evolution : Once QGP is formed, the medium has a pressure gradient. The pressure gradient drives the cooling and expansion of the medium to achieve equilibrium. Relativistic hydrodynamic flow explains the expansion of the medium. QGP consists of deconfined quarks and gluons, strongly coupled to its neighbors, and behaves like a near-perfect liquid with specific viscosity ($\eta/s \approx 0.16$)[22]. The time scale of expansion can be estimated by the size of the fireball and the speed of sound in the medium. The approximate time scale for expansion is 10 fm/c in the lab frame.

4. Hadronization : As QGP evolves, it cools down by expansion. An expansion of QGP leads to lower energy density. Once QGP reaches the temperature of 100-200 MeV with an energy density of less than hadron, quarks and gluons recombine and form hadronic gas, a process known as chemical freeze-out. Chemical freeze-out has been observed around 155 MeV in different experiments at LHC and RHIC.[3][1]After Chemical freeze-out, hadronic gas continues to interact elastically and expand until it reaches kinetic freeze-out, leading to finalizing momenta of final state particles. The time scale of the stage can be calculated from the String Model or Coalescence Model.

5. Final State : The final states of particles are fixed with fixed momentum. The particles travel outwards, eventually reaching the detector. An event vertex is constructed with tracks left behind by the particles in the detector.

2 Detectors and Accelerator

Extreme energy required to produce QGP can be achieved by accelerating heavy ions in particle accelerators at relativistic speeds. Accelerator facilities like Relativistic Heavy-ion Collider (RHIC) (Figure 4a) situated at Brookhaven National Lab and Large Hadron Collider (LHC)(Figure 4b) situated at CERN can produce QGP in heavy ion collisions like PbPb, pPb, and AuAu.

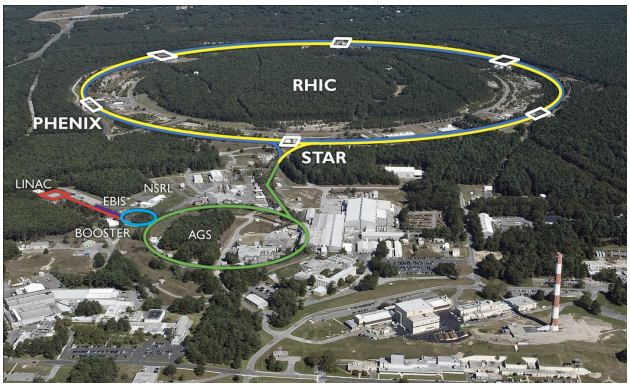

(a) Relativistic Heavy-ion Collider

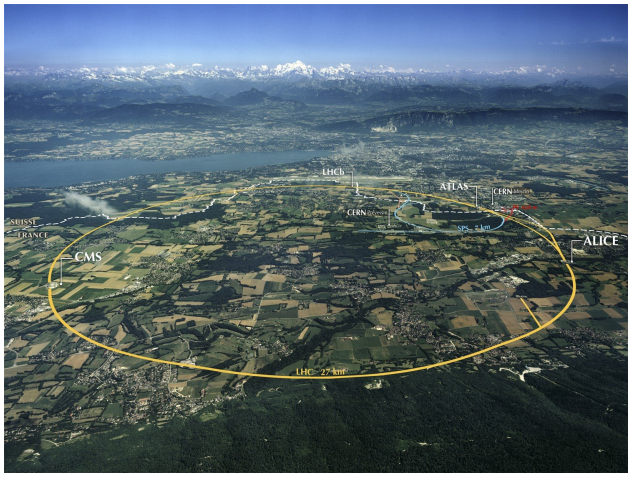

(b) Large Hadron Collider

Figure 4: Particle Accelerators

2.1 Detector Geometry

Detectors are built in cylindrical shape. Cylindrical shape warrants the use of cylindrical coordinates for observables. In detectors, beams travel along the z-axis with azimuthal angle (ϕ) spanning the transverse plane perpendicular to the beam axis. Detectors are very limited in terms of what quantities can be detected.

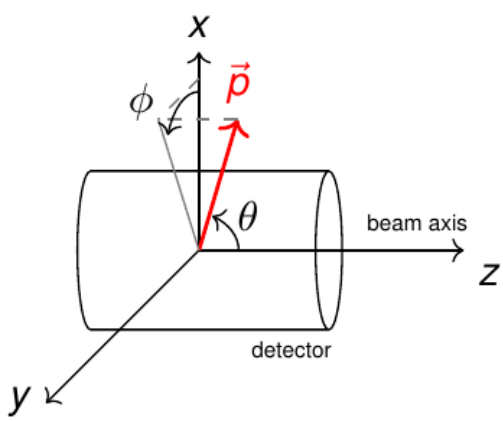

(a) Geometry of Detector

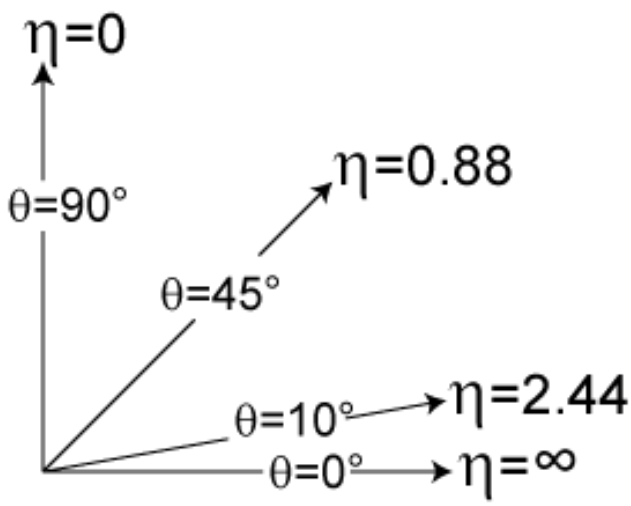

(b) Conversion of pseudorapidity (η) to polar angle (θ)

Measuring polar angle is difficult. Instead of a polar angle, a related quantity rapidity (y) is defined below

$$y = \frac{1}{2} \ln \left(\frac{E + p_z}{E - p_z} \right)$$

Rest mass (M) of particle and total energy (E) of particle, in natural units $\hbar = c = 1$, are related as follows

$$E^2 = p^2 + M^2$$

Detectors can not measure the total energy of particles directly. However, measuring particles' momentum is possible when particles travel through the uniform magnetic field (B). When the momentum of a particle is large compared to the rest mass, rapidity (y) can be converted into pseudorapidity (η) as follows

$$y = \frac{1}{2} \ln \left(\frac{p + p_z}{p - p_z} \right)$$

Pseudorapidity is Lorentz-invariant for particles with zero rest mass. Pseudorapidity can be converted to the polar angle as follows

$$\eta = -\ln \left[\tan \left(\frac{\theta}{2} \right) \right]$$

The polar angle in the detector can not span for 0 to π. Detectors are built with a fixed range of pseudorapidity. CMS detector tracker has pseudorapidity acceptance between $-2.4 < \eta < 2.4$. Figure 5(b) shows the conversion of pseudorapidity (η) to a polar angle (θ)

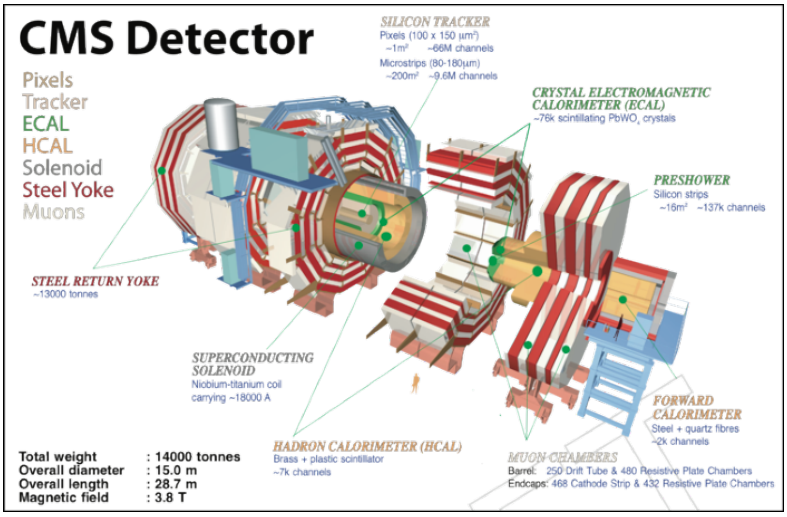

Figure 6: CMS Detector

3 Signatures of QGP

QGP can not be probed directly because of its extremely short-lived lifetime. However, different signatures of QGP can be studied. In this section, some of these signatures are described.

3.1 Glauber Model

In ultrarelativistic heavy ion collisions, when two nuclei collide head-on, it produces events with large charge particle multiplicities. Multiplicity varies from a few particles to thousands of particles, depending on the overlap of two nuclei. Events with different multiplicities can not be studied together because of different amounts of overlap. Figure 7(a) shows an AuAu collision with an ions overlap. It is impossible to measure the overlap of nuclei directly. However, a theoretical framework known as the Glauber Model is available to estimate the overlap. To estimate impact parameter (b), the number of participating nucleons (N_{part}), and binary nucleon-nucleon collisions, the Galuber model relies on Monte Carlo simulation. Initially, each nucleon is assigned a position stochastically inside the nucleus. Nuclei collide under the assumption that nucleons travel in a straight line along the beam and that the inelastic nucleon-nucleon cross-section is independent of the number of collisions a nucleon has undergone before. Impact parameter b is then drawn from the distribution $d\sigma/db = 2\pi b$. Two nuclei collide if the distance is

$$d \leq \sqrt{\sigma_{\text{inel}}^{\text{NN}}/\pi}$$

where $\sigma_{\text{inel}}^{\text{NN}}$ is the total inelastic nucleon-nucleon cross-section. Systematic studies show depen-

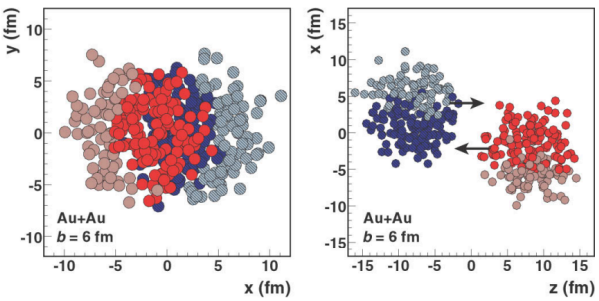

(a) AuAu collision. Dark nucleons are participating (N_{part}) nucleons.

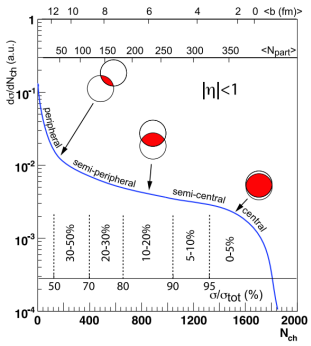

(b) A cartoon example of correlation of N_{ch} and Glauber calculated quantities (b, N_{part})

Figure 7

dence of N_{part} and N_{coll} on the size of system.[21] In a collision of two same nuclei the number of collisions follows

$$N_{\text{coll}} \propto N_{\text{part}^{4/3}}$$

independent of the size of nuclei. To classify events in specific centrality classes, it is assumed that charge particle multiplicity monotonically decreases with an increase in impact parameters. Charged particle multiplicity N_{ch} is measured for Monte-Carlo generated events and events in the experiment. Centrality class is defined as the fraction of total events.(Figure 7(b))

3.2 Strangeness Enhancement

Particle yield ratios relative to pions increase with multiplicity in pp and pPb collisions. In heavy ion collisions, the ratio remains constant, as shown in Figure 8a. These ratios are independent of the center of mass energy. This is an indication that hadron yields depend on final

state-charged particle multiplicity. The rate of production of strange particles increases rapidly with multiplicity compared to particles containing light quarks, u, and d. This increase in the production of strange particles is known as strangeness enhancement.

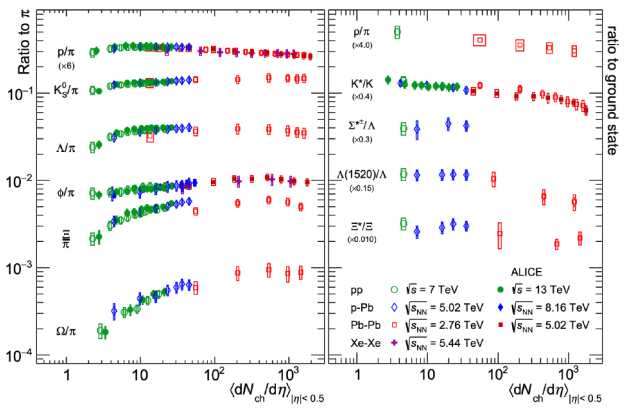

(a) p_T integrated ratios to pions (left) and p_T integrated yield ratios between resonances and ground states[2]

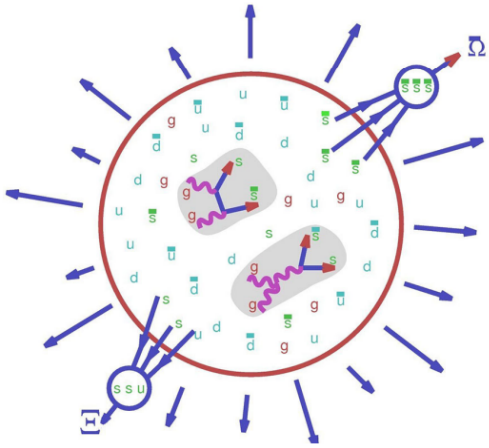

(b) A cartoon example of strange particle formation from QGP

Figure 8

Strangeness enhancement can be explained by the higher production of strange baryons in high multiplicity events. In QGP, partons with an energy of a few hundred MeV lead to the formation of strange baryons. In a freeze-out stage, a higher abundance of strange baryons contributes to the enhanced production of particles with strange baryon content, as shown in Figure 8b. This phenomenon was first observed by the ALICE collaboration. [2]

3.3 Heavy quarkonia suppression

Finite temperature lattice QCD calculations suggest the phase transition from hadronic matter to QGP at a critical temperature of around 155 MeV. Heavy quarks prove to be valuable probes for studying the characteristics of QGP medium. The mass of heavy quarks is significantly higher than the plasma temperature and Λ_{QCD}. Heavy quark production time is much shorter than QGP lifetime. This makes a heavy quark out of equilibrium probe. At extremely high temperatures and densities, strongly interacting matter goes through a transition, allowing quarks and gluons to be "free," a phenomenon known as deconfinement. In the presence of a free color charge, the Debey-Hiiickel type screening weakens the strong interaction. The quarkonium is a flavorless meson consisting of a pair of heavy quark and anti-quark. Quarkoniums like J/ψ and Υ are small compared to other reasons, providing them a chance to survive in QGP. However, "Debey screening" will weaken these tightly bound particles. The screening effect intensifies as temperature increases.

The color screening effect would dissociate the bound state of a $c\bar{c}$ and $b\bar{b}$ in the QGP medium at sufficiently higher temperatures, suppressing charmonium and bottomonium production.[20] The binding energies of quarkonia vary from few MeV ($\psi(2S)$) to 1 GeV $\Upsilon(1S)$, suggests a "sequential suppression". Figure 9 shows the nuclear modification factor measured based on pp and PbPb data collected at the CMS experiment 2015.[24] The nuclear modification factor is defined as

$$R_{AA} = \frac{1}{T_{AA}} \frac{dN_{AA}/dp_T}{d\sigma_{pp}/dp_T} = \frac{1}{N_{coll}} \frac{dN_{AA}/dp_T}{dN_{pp}/dp_T}$$

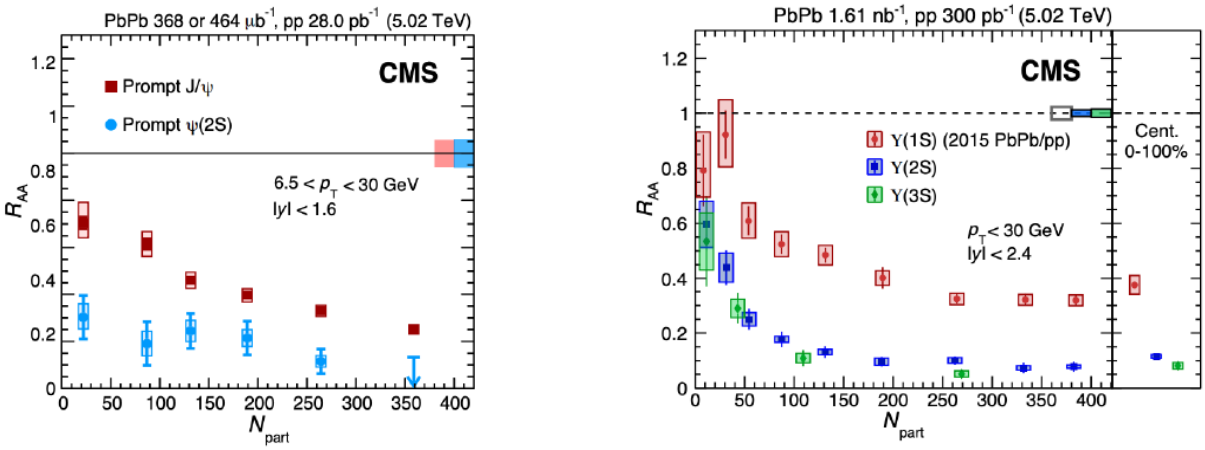

Figure 9: Nuclear Modification factors for promptly produced J/ψ, $\psi(2S)$ mesons (left)[24], $\Upsilon(1S)$, $\Upsilon(2S)$ and $\Upsilon(3S)$ (Right)[26]

3.4 Hydrodynamic Flow

The QGP behaves as an almost ideal liquid, implying that the initial spatial anisotropies could result in the final stage momentum configuration. These anisotropies arise from fluctuations in energy density or almond shape of the nuclei overlap region. The non-uniform energy density in the initial state creates a pressure gradient. The pressure gradient will drive the expansion of QGP. If the pressure gradient is larger than the mean free path, hydrodynamics flow explains the evolution of the system. Higher pressure at the center of QGP will result in outward radial flow. This continuous evolution of the system will be captured in the freeze-out stage in the form of particle density in the azimuthal angle ϕ. The dependence of particle density on the azimuthal angle is described by Fourier series expansion given by,

$$\frac{dN}{d\phi} \propto 1 + 2\sum_{n=1}^{\infty} v_n \cos[n(\phi - \Psi_n)]$$

The coefficient v_n is known as the anisotropic flow coefficient. v_1 Ψ_n is the reaction plane angle. Directed flow is quantified by first-order coefficient v_1 and elliptic flow is described by second-order coefficient v_2.

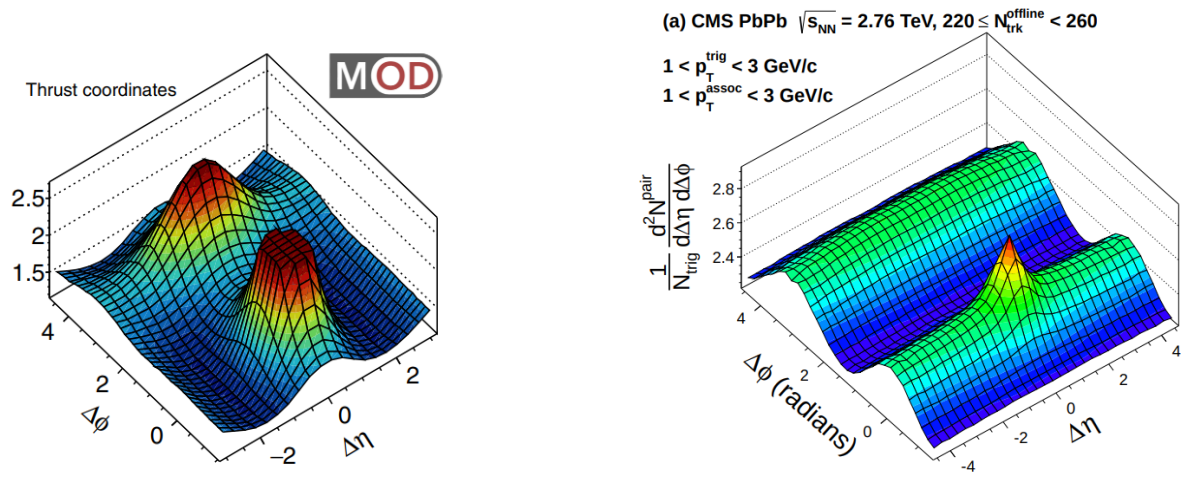

(a) Two particle correlation in e^-e^+ collision.[6]

(b) Two particle correlation in Pb-Pbcollision.[10]

Figure 10

The coefficients are obtained by fitting a Fourier function to $\Delta\phi$ histogram obtained by projection from 2D $(\Delta\eta, \Delta\phi)$ histogram. The near side ridge observed at large $\Delta\eta$ in Figure 10(b), is a result of elliptic and higher order flow, confirming the presence of QGP. The ridge is absent in case of electron positron collision shown in Figure 10(a)

3.5 Jets

In a heavy ion collision, jets are formed when a parton in a nucleon scatters off from a parton in another nucleon, leading to the parton shower. The parton shower hadronizes into a collimated spray of hadrons known as jets. The majority of the hard scatterings are $2 \to 2$, meaning jets will be produced in the pair approximately 180° apart in the azimuthal plane. The formation and evolution of jets in vacuum have been studied in e^-e^+, e^-p, and pp collisions at various colliders.[13][15][4]. Jets are parametrized by the jet cone radius and reconstructed using different computational algorithms like the k_T algorithm[14], the anti-k_T algorithm[9], etc.

3.5.1 Jet Quenching and Jet Suppression

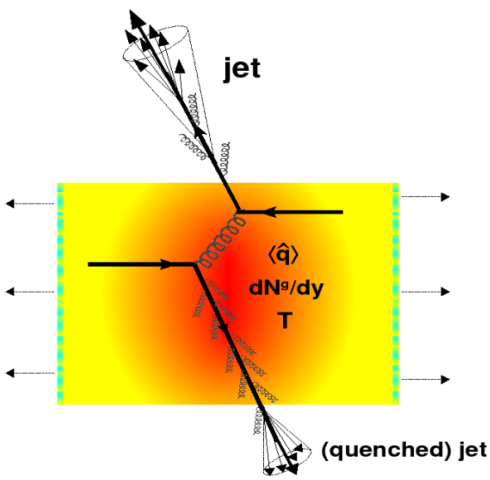

(a) A cartoon illustration of a dijet production where one parton traverses through a medium[12]

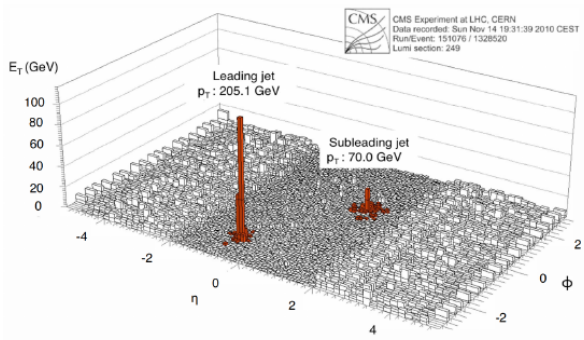

(b) A dijet event with unbalanced momentum in PbPb collision event at $\sqrt{S_{\mathrm{NN}}} = 2.76$ TeV, recorded at CMS [11]

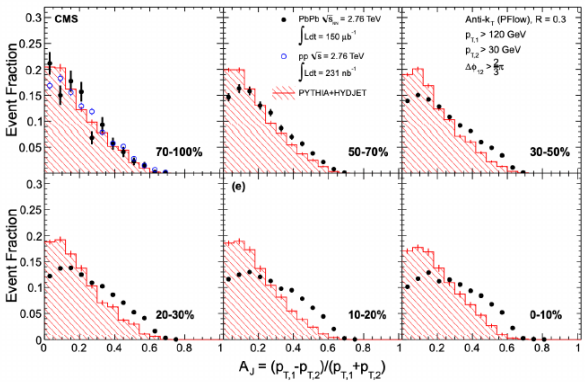

(c) A_J distribution for a jet pair with the leading jet transverse momentum $p_{T,1} > 120$ GeV and subleading jet transverse momentum $p_{T,2} > 30$ GeV with azimuthal angle difference of $2\pi/3$ [11]

Figure 11

In the presence of QGP, one of the partons has to traverse through the medium (Figure 11(a)),

losing energy due to interaction with the medium, leading to momentum imbalance between jets. This phenomenon of loss of energy is called "jet quenching". The parton loses energy by the radiative process and the scattering in the medium. The nuclear modification factor for jets in heavy ion collision AA as compared to pp collision is defined as

$$R_{\mathrm{AA}}^{\mathrm{jet}} = \frac{dN_{\mathrm{jet}}^{\mathrm{AA}}/dp_T}{\langle N_{\mathrm{coll}}\rangle\, dN_{\mathrm{jet}}^{\mathrm{pp}}/dp_T}$$

Asymmetric suppression of the transverse momentum in the dijet event is expected because of energy loss experienced by the parton. Jet transverse momentum imbalance between the leading jet and the sub-leading jet is a sign of jet quenching shown in Figure 11(c)[11], quantified by dijet-asymmetry

$$A_j = \frac{p_{T,1} - p_{T,2}}{p_{T,1} + p_{T,2}}$$

3.5.2 Jet Shapes

The energy lost by the parton inside QGP is recovered in the form of soft hadrons at a larger angular distance from the jet axis. Particle distribution inside the jet cone is studied by jet shape and jet fragmentation. Jet shape is defined as transverse momentum weighted distribution of particles around the jet axis.

$$\rho(\Delta r) = \frac{1}{(\delta r) N_{\mathrm{jets}}} \sum_{\mathrm{jets}} \frac{\sum_{\mathrm{tracks}\in[r_a,r_b)} p_T^{\mathrm{ch}}}{p_T^{\mathrm{jet}}}$$

In the presence of QGP, the parton energy loss will broaden the jet, pushing the matter out of the jet from the side of the jet cone as shown in Figure 12.[23]

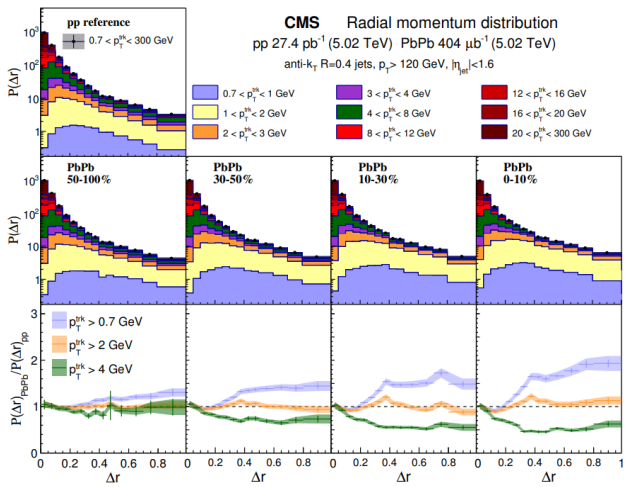

Figure 12: Jet shapes distribution for pp and different centrality for PbPb

4 Small systems and QGP

The evidence of the formation of QGP in heavy ions like PbPb and AuAu has been extensively proven by the study of quarkonia suppression, strangeness enhancement, jet quenching, etc. However, since 2010 different signatures of QGP have been observed in pp collision and pPb collisions. [18][19][25]. These results have ignited the curiosity to check if the QGP will be formed in small systems. However, there has been no result of jet quenching present in small systems so far. I will be focusing my effort on quantifying the jet quenching in pPb collisions at $\sqrt{s_{\mathrm{NN}}} = 8.16$ TeV.

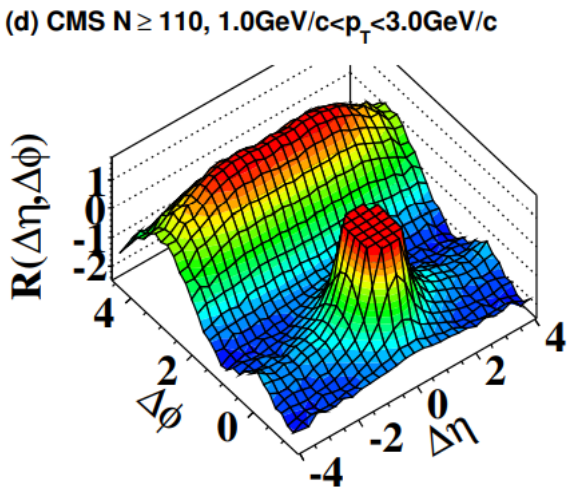

(a) 2D Particle correlation for 7TeV pp for high multiplicity ($N_{trk}^{offline} \geq 110$) events with $1 < p_T < 3$ GeV/c. [19]

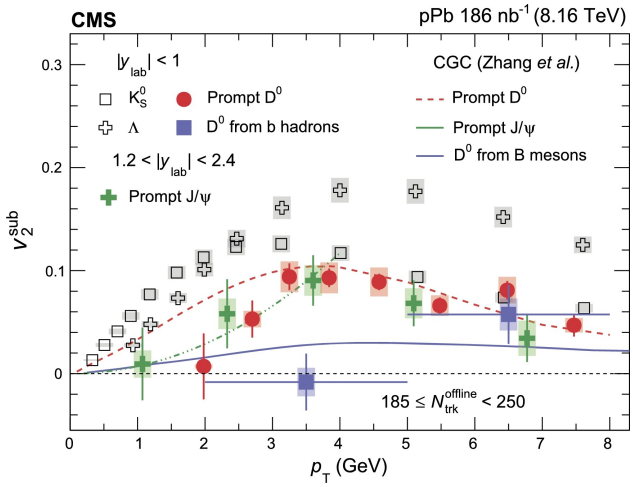

(b) Results of v_2^{sub} for prompt and nonprompt D^0 mesons, as well as K_S^0 mesons, Λbaryons for $|y_{lab}| < 1$, and prompt J/ψ mesons for $1.2 < |y_{lab}| < 2.4$, as functions of pT.[25]

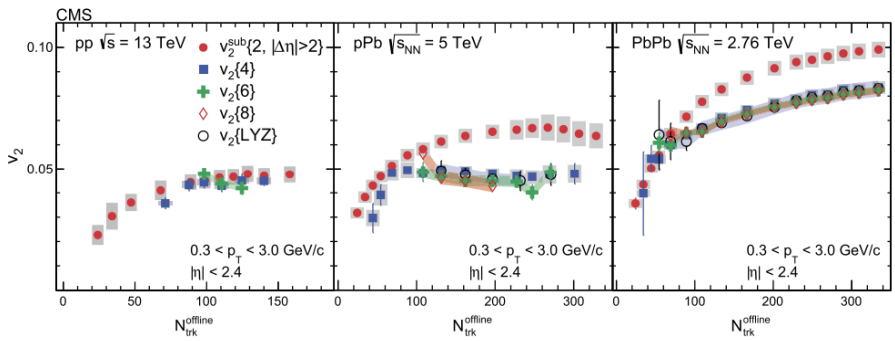

(c) Measured collective behavior (v_2) in different collision systems [18]

Figure 13

References

[1] B. Abelev et al. "Centrality dependence of π, K, and p production in Pb-Pb collisions at $\sqrt{s_{NN}} = 2.76$ TeV". In: *Phys. Rev. C* 88 (4 Oct. 2013), p. 044910. DOI: 10.1103/PhysRevC.88.044910. URL: https://link.aps.org/doi/10.1103/PhysRevC.88.044910.

[2] J. Adam et al. "Enhanced production of multi-strange hadrons in high-multiplicity proton–proton collisions". In: *Nature Physics* 13.6 (Apr. 2017), pp. 535–539. ISSN: 1745-2481. DOI: 10.1038/nphys4111. URL: http://dx.doi.org/10.1038/nphys4111.

[3] L. Adamczyk et al. "Bulk properties of the medium produced in relativistic heavy-ion collisions from the beam energy scan program". In: *Physical Review C* 96.4 (Oct. 2017). ISSN: 2469-9993. DOI: 10.1103/physrevc.96.044904. URL: http://dx.doi.org/10.1103/PhysRevC.96.044904.

[4] G. Altarelli and G. Parisi. "Asymptotic freedom in parton language". In: *Nuclear Physics B* 126.2 (1977), pp. 298–318. ISSN: 0550-3213. DOI: https://doi.org/10.1016/0550-3213(77)90384-4. URL: https://www.sciencedirect.com/science/article/pii/0550321377903844.

[5] M. Arslandok et al. *Hot QCD White Paper*. 2023. arXiv: 2303.17254 [nucl-ex]. URL: https://arxiv.org/abs/2303.17254.

[6] Anthony Badea et al. "Measurements of Two-Particle Correlations in e^+e^- Collisions at 91 GeV with ALEPH Archived Data". In: *Phys. Rev. Lett.* 123 (21 Nov. 2019), p. 212002. DOI: 10.1103/PhysRevLett.123.212002. URL: https://link.aps.org/doi/10.1103/PhysRevLett.123.212002.

[7] A. Bazavov et al. "Equation of state in (2+1)-flavor QCD". In: *Physical Review D* 90.9 (Nov. 2014). ISSN: 1550-2368. DOI: 10.1103/physrevd.90.094503. URL: http://dx.doi.org/10.1103/PhysRevD.90.094503.

[8] J. D. Bjorken. "Highly relativistic nucleus-nucleus collisions: The central rapidity region". In: *Phys. Rev. D* 27 (1 Jan. 1983), pp. 140–151. DOI: 10.1103/PhysRevD.27.140. URL: https://link.aps.org/doi/10.1103/PhysRevD.27.140.

[9] Matteo Cacciari, Gavin P Salam, and Gregory Soyez. "The anti-ktjet clustering algorithm". In: *Journal of High Energy Physics* 2008.04 (Apr. 2008), pp. 063–063. ISSN: 1029-8479. DOI: 10.1088/1126-6708/2008/04/063. URL: http://dx.doi.org/10.1088/1126-6708/2008/04/063.

[10] S. Chatrchyan et al. "Multiplicity and transverse momentum dependence of two- and four-particle correlations in pPb and PbPb collisions". In: *Physics Letters B* 724.4–5 (July 2013), pp. 213–240. ISSN: 0370-2693. DOI: 10.1016/j.physletb.2013.06.028. URL: http://dx.doi.org/10.1016/j.physletb.2013.06.028.

[11] S. Chatrchyan et al. "Observation and studies of jet quenching in PbPb collisions at $\sqrt{s_{NN}} = 2.76$ TeV". In: *Phys. Rev. C* 84 (2 Aug. 2011), p. 024906. DOI: 10.1103/PhysRevC.84.024906. URL: https://link.aps.org/doi/10.1103/PhysRevC.84.024906.

[12] David d'Enterria. "6.4 Jet quenching". In: *Relativistic Heavy Ion Physics*. Springer Berlin Heidelberg, 2010, pp. 471–520. ISBN: 9783642015397. DOI: 10.1007/978-3-642-01539-7_16. URL: http://dx.doi.org/10.1007/978-3-642-01539-7_16.

[13] Yuri L. Dokshitzer. "Calculation of the Structure Functions for Deep Inelastic Scattering and e+ e- Annihilation by Perturbation Theory in Quantum Chromodynamics." In: *Sov. Phys. JETP* 46 (1977), pp. 641–653.

[14] Stephen D. Ellis and Davison E. Soper. "Successive combination jet algorithm for hadron collisions". In: *Physical Review D* 48.7 (Oct. 1993), pp. 3160–3166. ISSN: 0556-2821. DOI: 10.1103/physrevd.48.3160. URL: http://dx.doi.org/10.1103/PhysRevD.48.3160.

[15] V.N. Gribov and L.N. Lipatov. "Deep inelastic electron scattering in perturbation theory". In: *Physics Letters B* 37.1 (1971), pp. 78–80. ISSN: 0370-2693. DOI: https://doi.org/10.1016/0370-2693(71)90576-4. URL: https://www.sciencedirect.com/science/article/pii/0370269371905764.

[16] Particle Data Group et al. "Review of Particle Physics". In: *Progress of Theoretical and Experimental Physics* 2022.8 (Aug. 2022), p. 083C01. ISSN: 2050-3911. DOI: 10.1093/ptep/ptac097. eprint: https://academic.oup.com/ptep/article-pdf/2022/8/083C01/49175539/ptac097.pdf. URL: https://doi.org/10.1093/ptep/ptac097.

[17] Miklos Gyulassy. *The QGP Discovered at RHIC*. 2004. arXiv: nucl-th/0403032 [nucl-th]. URL: https://arxiv.org/abs/nucl-th/0403032.

[18] V. Khachatryan et al. "Evidence for collectivity in pp collisions at the LHC". In: *Physics Letters B* 765 (2017), pp. 193–220. ISSN: 0370-2693. DOI: https://doi.org/10.1016/j.physletb.2016.12.009. URL: https://www.sciencedirect.com/science/article/pii/S037026931630747X.

[19] V. Khachatryan et al. "Observation of long-range, near-side angular correlations in proton-proton collisions at the LHC". In: *Journal of High Energy Physics* 2010.9 (Sept. 2010). ISSN: 1029-8479. DOI: 10.1007/jhep09(2010)091. URL: http://dx.doi.org/10.1007/JHEP09(2010)091.

[20] T. Matsui and H. Satz. "J/ψ suppression by quark-gluon plasma formation". In: *Physics Letters B* 178.4 (1986), pp. 416–422. ISSN: 0370-2693. DOI: https://doi.org/10.1016/0370-2693(86)91404-8. URL: https://www.sciencedirect.com/science/article/pii/0370269386914048.

[21] Michael L. Miller et al. "Glauber Modeling in High-Energy Nuclear Collisions". In: *Annual Review of Nuclear and Particle Science* 57.1 (Nov. 2007), pp. 205–243. ISSN: 1545-4134. DOI: 10.1146/annurev.nucl.57.090506.123020. URL: http://dx.doi.org/10.1146/annurev.nucl.57.090506.123020.

[22] S. Ryu et al. "Importance of the Bulk Viscosity of QCD in Ultrarelativistic Heavy-Ion Collisions". In: *Phys. Rev. Lett.* 115 (13 Sept. 2015), p. 132301. DOI: 10.1103/PhysRevLett.115.132301. URL: https://link.aps.org/doi/10.1103/PhysRevLett.115.132301.

[23] A. M. Sirunyan et al. "Jet properties in PbPb and pp collisions at

$$\sqrt{s_{\mathrm{N\,N}}} = 5.02$$

TeV". In: *Journal of High Energy Physics* 2018.5 (May 2018). ISSN: 1029-8479. DOI: 10.1007/jhep05(2018)006. URL: http://dx.doi.org/10.1007/JHEP05(2018)006.

[24] A. M. Sirunyan et al. "Measurement of prompt and nonprompt charmonium suppression in PbPb collisions at 5.02 TeV". In: *The European Physical Journal C* 78.6 (June 2018). ISSN: 1434-6052. DOI: 10.1140/epjc/s10052-018-5950-6. URL: http://dx.doi.org/10.1140/epjc/s10052-018-5950-6.

[25] A.M. Sirunyan et al. "Studies of charm and beauty hadron long-range correlations in pp and pPb collisions at LHC energies". In: *Physics Letters B* 813 (2021), p. 136036. ISSN: 0370-2693. DOI: https://doi.org/10.1016/j.physletb.2020.136036. URL: https://www.sciencedirect.com/science/article/pii/S037026932030839X.

[26] A. Tumasyan et al. "Observation of the $\Upsilon(3S)$ Meson and Suppression of Υ States in Pb-Pb Collisions at $\sqrt{s_{NN}} = 5.02$ TeV". In: *Phys. Rev. Lett.* 133 (2 July 2024), p. 022302. DOI: 10.1103/PhysRevLett.133.022302. URL: https://link.aps.org/doi/10.1103/PhysRevLett.133.022302.